Orthogonality breaking sensing model based on the instantaneous Stokes vector and the Mueller calculus

Noé Ortega-Quijano,[1,*] Julien Fade,[1] Muriel Roche,[2] François Parnet,[1] and Mehdi Alouini[1]

[1] *Institut de Physique de Rennes, CNRS, Université de Rennes 1, Campus de Beaulieu, 35 042 Rennes, France*

[2] *Aix-Marseille Université, CNRS, Centrale Marseille, Institut Fresnel, UMR 7249, 13 013 Marseille, France*

arXiv:1512.02401v1 [physics.optics] 8 Dec 2015

compiled: December 9, 2015

Polarimetric sensing by orthogonality breaking has been recently proposed as an alternative technique for performing direct and fast polarimetric measurements using a specific dual-frequency dual-polarization (DFDP) source. Based on the instantaneous Stokes-Mueller formalism to describe the high-frequency evolution of the DFDP beam intensity, we thoroughly analyze the interaction of such a beam with birefringent, dichroic and depolarizing samples. This allows us to confirm that orthogonality breaking is produced by the sample diattenuation, whereas this technique is immune to both birefringence and diagonal depolarization. We further analyze the robustness of this technique when polarimetric sensing is performed through a birefringent waveguide, and the optimal DFDP source configuration for fiber-based endoscopic measurements is subsequently identified. Finally, we consider a stochastic depolarization model based on an ensemble of random linear diattenuators, which makes it possible to understand the progressive vanishing of the detected orthogonality breaking signal as the spatial heterogeneity of the sample increases, thus confirming the insensitivity of this method to diagonal depolarization. The fact that the orthogonality breaking signal is exclusively due to the sample dichroism is an advantageous feature for the precise decoupled characterization of such an anisotropic parameter in samples showing several simultaneous effects.

OCIS codes: (110.5405) Polarimetric imaging, (120.5410) Polarimetry, (260.2130) Ellipsometry and polarimetry, (100.1930) Dichroism

http://dx.doi.org/10.1364/XX.99.099999

1. Introduction

Polarimetric imaging systems are of growing interest for many applications like remote sensing [1], astronomy [2], defense [3, 4], biomedicine [5–8], synthetic-aperture radar [9], and machine or enhanced vision [10, 11]. Active polarimetric techniques allow valuable information of a given scene or sample to be retrieved from the measure of its anisotropic and depolarizing properties. Mueller polarimetry is the most exhaustive active technique, as it completely characterizes the polarimetric parameters of an object. This technique typically implies registering 16 images using different approaches to modulate the measurement in the spatial, temporal, and/or spectral domain [12–17]. However, the complexity of the system and the loss of performance entailed by the different multiplexing methods have led to propose several simplified polarimetric techniques which optimize the measurement of some specific polarimetric properties at a high performance [18–21].

In this context, the implementation of fiber-guided polarimetric imaging systems constitutes a challenging issue, due to the fact that the state of polarization of the illuminating beam is modified by the optical waveguide in an uncontrolled way. This is a remarkable aspect to be adressed for endoscopic applications, where the optical fiber stress-induced birefringence is the dominant effect on beam polarization [22]. The feasibility of a multimodal endoscopic system including cross-polarized imaging has been demonstrated for Barett's metaplasia imaging [23]. However, such a technique provides an orientation-dependent contrast, which entails some drawbacks for *in vivo* applications. Moreover, the fact that the polarimetric elements and the CCD camera are placed in the distal end of the endoscope is quite restrictive in terms of miniaturization. Regarding Mueller polarimetry, a narrow band 3×3 Mueller polarimetric endoscope was presented and validated *ex vivo* on a Sprague-Dawley rat [24]. However, the use of a rigid endoscope is unfeasible for most practical applications. Finally, a full Mueller endoscopic polarimeter, based on a first characterization of the optical fiber using a micro-switchable mirror before every Mueller matrix acquisition, was proposed in [25]. Recently, this novel technique has been combined with a spectral encoding of polarimetric channels to significantly reduce the acquisition time [26].

Recently, we proposed a novel polarimetric imaging modality based on the orthogonality breaking sensing principle [27]. This technique uses a dual-frequency dual-polarization (DFDP) coherent source, and is based

* Corresponding author: noe.ortega@univ-rennes1.fr

on the measurement of the detected intensity component at the radio-frequency beatnote after interaction with the sample or scene under analysis. This technique enables a subset of its polarimetric properties to be determined from a single acquisition at both high speed and high dynamic range. The first implementation of a polarimetric contrast microscope by orthogonality breaking was presented in [28]. A modified source architecture, enabling the linear diattenuation and optic axis of the sample to be completely characterized, was subsequently described and validated in [29]. Though insensitive to birefringence effects which are predominant in biological tissues, this technique provides an alternative method to characterize biological anisotropic structures. Indeed, biological tissues usually show both birefringence and dichroism sharing the same anisotropy axis [30, 31]. As a result, biological anisotropic structures can nonetheless be addressed by measuring their diattenuation properties, provided the measurement dynamics is high enough. However, all these previous works on orthogonality breaking imaging [27–29] were focused on specific examples and particular measurement configurations. The in-depth analysis of the physical origin of the orthogonality breaking signal amplitude and phase, in relation with the polarimetric properties of the sample and the characteristics of the illumination system, is still an open question.

In this work, we develop a comprehensive theoretical model of orthogonality breaking sensing based on the instantaneous Stokes vector and the Mueller calculus. This approach makes it possible to describe the interaction of the DFDP beam with anisotropic depolarizing samples. Based on this method, we develop a thorough analysis of the orthogonality breaking signal characteristics for both free-space and fiber-guided measurements. The results are presented for the basic types of optical elements, namely isotropic absorbers, elliptical, circular, and linear retarders and diattenuators, and diagonal depolarizers. This theoretical analysis is then completed with a detailed discussion, based on both simulations and experimental measurements, which allows us to conclude that the orthogonality-breaking technique is definitely not sensitive to diagonal depolarization. Throughout this work, a special emphasis is made on the practical implications of each configuration for experimental polarimetry.

This paper is organized as follows: the instantaneous Stokes vector description of a polarized light beam is reviewed in Section 2, before applying it to the specific characterization of the DFDP source in Section 3. Using the instantaneous Stokes-Mueller formalism, we then thoroughly study in Section 4 how this type of laser source can be used for free-space polarimetric sensing by the orthogonality breaking principle. The influence of an optical waveguide on orthogonality breaking sensing is then investigated in Section 5 to analyze the potential of this technique for endoscopic applications. Lastly, a discussion on the sensitivity of this technique to depolarization is presented in Section 6 using a stochastic model of linear diattenuation with random optic axis orientation, before the conclusion of this work is given in Section 7.

2. Instantaneous Stokes vector

Firstly, we consider a fluctuating optical plane wave described by its transverse electric field. The reference frame is set so that propagation is along the z axis in a right-handed Cartesian coordinate system xyz, and thus the complex electric field at a specific point z_0 can be resolved into a pair of orthogonal polarization states:

$$\vec{\mathbf{E}}(t) = \begin{bmatrix} E_1(t) \\ E_2(t) \end{bmatrix}. \tag{1}$$

The corresponding instantaneous Stokes vector is a 4-element real vector

$$\vec{\mathbf{S}}(t) = \begin{bmatrix} S_0(t) \\ S_1(t) \\ S_2(t) \\ S_3(t) \end{bmatrix} \tag{2}$$

whose elements are the instantaneous Stokes parameters, defined in terms of the complex electric field components as [32]:

$$S_0(t) = E_1(t)E_1^*(t) + E_2(t)E_2^*(t), \tag{3}$$
$$S_1(t) = E_1(t)E_1^*(t) - E_2(t)E_2^*(t), \tag{4}$$
$$S_2(t) = E_1(t)E_2^*(t) + E_1^*(t)E_2(t), \tag{5}$$
$$S_3(t) = i\left[E_1(t)E_2^*(t) - E_1^*(t)E_2(t)\right]. \tag{6}$$

The first component $S_0(t) = \vec{\mathbf{E}}(t)^\dagger \vec{\mathbf{E}}(t)$ is the instantaneous intensity of the field, with † denoting the Hermitian conjugate.

The instantaneous Stokes vector completely characterizes the state of polarization (SOP) of a partially polarized light beam, except its absolute phase. The conventional Stokes parameters are the ensemble averages of the instantaneous Stokes parameters. Assuming stationarity and ergodicity, the conventional Stokes vector is :

$$\vec{\mathbf{S}} = \langle \vec{\mathbf{S}}(t) \rangle = \begin{bmatrix} \langle S_0(t) \rangle \\ \langle S_1(t) \rangle \\ \langle S_2(t) \rangle \\ \langle S_3(t) \rangle \end{bmatrix}, \tag{7}$$

which involves the following time average:

$$\langle X(t) \rangle = \lim_{T \to \infty} \frac{1}{T} \int_0^T X(t) \mathrm{d}t. \tag{8}$$

It is worth to recall that the conventional Stokes parameters are defined in this way simply because in most experimental setups the fluctuations of the electric field are produced at optical frequencies, which are obviously many orders of magnitude higher than those achievable by the fastest photodetector (so far, ultrafast optical

measurements can only be performed by specific techniques like nonlinear optical gating or interferometric detection, which are able to indirectly measure light intensity as well as its time delay). However, in the next section it is shown that the instantaneous Stokes vector is a very useful way to characterize DFDP sources.

3. Dual-frequency dual-polarization source

3.A. General equations

Assuming a dual-frequency dual-polarization (DFDP) source whose two orthogonal modes propagate along the z axis, its transversal electric field can be expressed as:

$$\vec{\mathbf{E}}(t) = \frac{E_0}{\sqrt{2}} e^{-i2\pi\nu t} \left(\begin{bmatrix} a_1 \\ b_1 \end{bmatrix} + \sqrt{\gamma} e^{-i2\pi\Delta\nu t} \begin{bmatrix} a_2 \\ b_2 \end{bmatrix} \right), \quad (9)$$

where $\Delta\nu$ is the frequency shift between both modes, and γ accounts for a possible intensity unbalancing between them. Taking into account the orthogonality condition between the SOP's of the two polarization modes, the components a_i and b_i in the cartesian basis can be parameterized in the following general form:

$$\begin{aligned} a_1 &= \cos\alpha\cos\epsilon - i\sin\alpha\sin\epsilon, \\ b_1 &= \sin\alpha\cos\epsilon + i\cos\alpha\sin\epsilon, \end{aligned} \quad (10)$$

and

$$\begin{aligned} a_2 &= -\sin\alpha\cos\epsilon + i\cos\alpha\sin\epsilon, \\ b_2 &= \cos\alpha\cos\epsilon + i\sin\alpha\sin\epsilon, \end{aligned} \quad (11)$$

where α is the polarization ellipse azimuth and ϵ is its ellipticity [32]. These equations verify the polarization orthogonality condition $a_1 a_2^* + b_1 b_2^* = 0$. We set $\alpha = 0$ without loss of generality, as we later consider optical elements with arbitrary azimuth. From Eqs. (2-6), the instantaneous Stokes vector of a general DFDP source is:

$$\vec{\mathbf{S}}(t) = I_0 \begin{bmatrix} 1 \\ \frac{1-\gamma}{1+\gamma}\cos(2\epsilon) - 2\frac{\sqrt{\gamma}}{1+\gamma}\sin(2\epsilon)\sin(\Delta\omega t) \\ 2\frac{\sqrt{\gamma}}{1+\gamma}\cos(\Delta\omega t) \\ \frac{1-\gamma}{1+\gamma}\sin(2\epsilon) + 2\frac{\sqrt{\gamma}}{1+\gamma}\cos(2\epsilon)\sin(\Delta\omega t) \end{bmatrix}, \quad (12)$$

where $I_0 = |\vec{\mathbf{E}}(t)|^2 = (1+\gamma)E_0^2/2$ and with $\Delta\omega = 2\pi\Delta\nu$ denoting the angular frequency that corresponds to the interference between both modes. The frequency shift $\Delta\nu$ can be tuned to values within the radio-frequency (RF) range, typically from several MHz up to tens of GHz. It can be observed that the instantaneous intensity $S_0(t)$ of this DFDP illumination is constant and equal to I_0.

3.B. Linear and circular DFDP source

On the one hand, if the DFDP source provides two purely-linear orthogonal SOP's, then $\epsilon = 0$ and the instantaneous Stokes vector is:

$$\vec{\mathbf{S}}_{\mathbf{L}}(t) = I_0 \begin{bmatrix} 1 \\ \frac{1-\gamma}{1+\gamma} \\ 2\frac{\sqrt{\gamma}}{1+\gamma}\cos(\Delta\omega t) \\ 2\frac{\sqrt{\gamma}}{1+\gamma}\sin(\Delta\omega t) \end{bmatrix}. \quad (13)$$

Moreover, if a perfectly balanced source is used ($\gamma = 1$), $\vec{\mathbf{S}}_{\mathbf{L}}(t)$ simplifies to:

$$\vec{\mathbf{S}}_{\mathbf{L}}(t) = I_0 \begin{bmatrix} 1 \\ 0 \\ \cos(\Delta\omega t) \\ \sin(\Delta\omega t) \end{bmatrix}, \quad (14)$$

which corresponds to an instantaneous Stokes vector continuously oscillating at an angular frequency $\Delta\omega$ from a linear $\pm 45°$ SOP to a purely circular one, as shown in the Poincaré sphere representation included in Fig. 1.a.

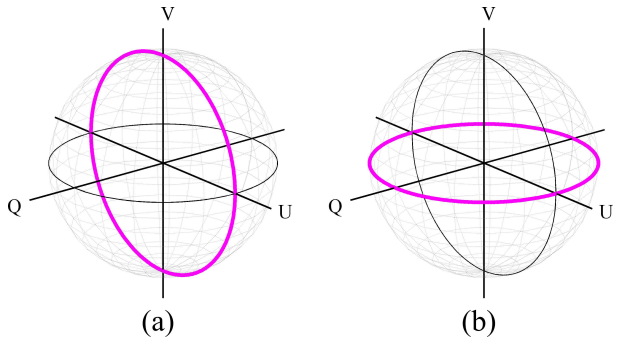

(a) (b)

Fig. 1. Poincaré sphere representation of the instantaneous Stokes vector at the output of the (a) linear DFDP (dual-frequency dual-polarization) balanced source, and (b) circular DFDP balanced source.

On the other hand, if we consider a circular DFDP source, $\epsilon = \pi/4$ and the instantaneous Stokes vector is given by:

$$\vec{\mathbf{S}}_{\mathbf{C}}(t) = I_0 \begin{bmatrix} 1 \\ -2\frac{\sqrt{\gamma}}{1+\gamma}\sin(\Delta\omega t) \\ 2\frac{\sqrt{\gamma}}{1+\gamma}\cos(\Delta\omega t) \\ \frac{1-\gamma}{1+\gamma} \end{bmatrix}, \quad (15)$$

which reduces to the following expression for a balanced source:

$$\vec{\mathbf{S}}_{\mathbf{C}}(t) = I_0 \begin{bmatrix} 1 \\ -\sin(\Delta\omega t) \\ \cos(\Delta\omega t) \\ 0 \end{bmatrix}. \quad (16)$$

It can be observed that the latter instantaneous Stokes vector oscillates along all the possible linear SOP's, as depicted in Fig. 1.b. The advantages of each of these sources for polarimetric measurements are analyzed in the next sections.

4. Free-space orthogonality breaking sensing

In this section, we focus on free-space orthogonality breaking sensing, in which the source beam directly impinges on the sample. According to the Mueller calculus, the output Stokes vector $\vec{\mathbf{S}}_{\mathbf{out}}(t)$ after interaction with an anisotropic depolarizing medium is given by:

$$\vec{\mathbf{S}}_{\mathbf{out}}(t) = \mathbf{M}\vec{\mathbf{S}}_{\mathbf{in}}(t), \quad (17)$$

where $\mathbf{M}$ is the Mueller matrix of the sample and $\vec{\mathbf{S}}_{\mathbf{in}}(t)$ is the input Stokes vector. It is worth recalling that this equation is valid for both the instantaneous and the conventional Stokes vector. All the subsequent results assume that the propagation direction is kept constant, so the measurement is made in transmission. The procedure can be equivalently developed for the reverse direction (reflection or backscattering configuration) provided that $\mathbf{M}$ is replaced by its corresponding Mueller matrix for the reverse direction:

$$\hat{\mathbf{M}} = \mathbf{O}\mathbf{M}^{\mathrm{T}}\mathbf{O}^{-1}, \tag{18}$$

where $\mathbf{O} = \mathrm{diag}(1, 1, -1, 1)$ if the reversal coordinate system $\hat{x}\hat{y}\hat{z}$ is set as $\hat{x} = -x$, $\hat{y} = y$ and $\hat{z} = -z$ [32] (or alternatively $\hat{x} = x$, $\hat{y} = -y$ and $\hat{z} = -z$).

In the remainder of this paper we will focus on the study of the detected intensity signal $I_{out}(t)$, which is a linear combination of the input instantaneous Stokes vector determined by the first row of the Mueller matrix:

$$I_{out}(t) = \begin{bmatrix} \mathrm{M}_{11} & \mathrm{M}_{12} & \mathrm{M}_{13} & \mathrm{M}_{14} \end{bmatrix} \vec{\mathbf{S}}_{\mathbf{in}}(t). \tag{19}$$

4.A. Isotropic absorber

The Mueller matrix of an isotropic absorber is the identity matrix weighted by the isotropic absorption coefficient ρ such that $\mathbf{M}_{\mathbf{abs}} = \rho\mathbf{I}$, and hence the output intensity is simply $I_{out}(t) = \rho I_0$. In this trivial case, it is straighforward to verify that the orthogonality between the two SOP's generated by a general DFDP source is unaltered by the sample, and consequently the measured intensity remains constant in time.

4.B. Elliptical retarder

A sample with elliptical birefringence presents a Mueller matrix of the following form [33]

$$\mathbf{M}_{\mathbf{ER}} = \begin{bmatrix} 1 & \vec{0}^{\mathrm{T}} \\ \vec{0} & \mathbf{M}_{3\times3} \end{bmatrix}, \tag{20}$$

where $\mathbf{M}_{3\times3}$ is the 3×3 retardance sub-matrix, and $\vec{0} = [0\ 0\ 0]^T$. It can be readily observed that the beam intensity is unaltered by such a type of sample:

$$I_{out}(t) = I_0, \tag{21}$$

as expected for unitary polarization elements [32]. As a result, the polarimetric orthogonality between the two SOP's provided by the DFDP source is preserved during propagation through birefringent samples. This is the property that was originally used to make orthogonality breaking measurements insensitive to propagation through fibers.

4.C. Diagonal depolarizer

The general expression of the Mueller matrix of a diagonal depolarizer sample is [32]:

$$\mathbf{M}_{\mathbf{\Delta}} = \begin{bmatrix} 1 & 0 & 0 & 0 \\ 0 & P_{L1} & 0 & 0 \\ 0 & 0 & P_{L2} & 0 \\ 0 & 0 & 0 & P_C \end{bmatrix}. \tag{22}$$

Diagonal depolarizers are thus defined by the three depolarization parameters P_{L1}, P_{L2}, and P_C. Such depolarizers are the most usual ones. In the particular situation of isotropic linear depolarization (like the one produced by a turbid medium with randomly-located nearly spherical particles [34]) $P_{L1} = P_{L2}$. Furthermore, if completely homogeneous depolarization is assumed, the sample is usually called a pure depolarizer, and it can be quantified by a single parameter as $P_{L1} = P_{L2} = P_C$.

In any case, the elements of the first row of $\mathbf{M}_{\mathbf{\Delta}}$ satisfy $\mathrm{M}_{1\mathrm{j}} = 0$ for $j \neq 1$, so according to Eq. (19) such a sample does not modify the orthogonality of the two orthogonally-polarized SOP's, and the beam intensity is expected to remain constant in time as $I_{out}(t) = I_0$.

As a result, the instantaneous Stokes-Mueller calculus detailed in this article indicates that the orthogonality-breaking sensing principle is not able to provide a measurement of diagonal depolarization. This is in contradiction with what was claimed in an anterior work [27], and with some experimental results obtained in the same reference which actually seemed to corroborate the possibility of characterizing depolarization. This aspect is analyzed and discussed in detail in Section 6.

4.D. Diattenuator

4.D.1. Linear diattenuator

The Mueller matrix of a sample showing linear dichroism is:

$$\mathbf{M}_{\mathbf{LD}} = \rho \begin{bmatrix} 1 & d\cos(2\phi) & d\sin(2\phi) & 0 \\ d\cos(2\phi) & \frac{1+T}{2} + \frac{1-T}{2}\cos(4\phi) & \frac{1-T}{2}\sin(4\phi) & 0 \\ d\sin(2\phi) & \frac{1-T}{2}\sin(4\phi) & \frac{1+T}{2} - \frac{1-T}{2}\cos(4\phi) & 0 \\ 0 & 0 & 0 & T \end{bmatrix}, \tag{23}$$

where $\rho = (T_{max} + T_{min})/2$ accounts for the isotropic absorption, $d = (T_{max} - T_{min})/(T_{max} + T_{min})$ is the diattenuation coefficient, and $T = 2\left[T_{max}T_{min}\right]^{\frac{1}{2}}/(T_{max} + T_{min})$. Parameters T_{max} and $T_{min} \leq T_{max}$ are the maximum and minimum transmittances respectively, being both of them bounded between 0 and 1, so $0 \leqslant d \leqslant 1$. Finally, the parameter ϕ is the linear dichroism angle,

i.e., the azimuth of the maximum transmittance axis. We note that $\mathbf{M_{LD}}$ can be obtained from the Mueller matrix of an elliptical diattenuator (explicitly derived in Appendix A for the sake of generality) by setting $\epsilon = 0$. An ideal polarizer corresponds to a perfect linear dichroic sample showing $T_{max} = 1$ and $T_{min} = 0$, so $\rho = 1/2$, $d = 1$ and $T = 0$.

In this section and in the remainder of this article we will consider a perfectly balanced source ($\gamma = 1$). Indeed, the equations of the output intensity for a linear diattenuator using a non-balanced linear and circular DFDP source have been included in Appendix B for the sake of completeness, and they show that the balanced configuration is actually the most advantageous one for characterizing the sample properties with the highest dynamics.

According to Eq. (19), if a linear diattenuator is illuminated with a balanced linear DFDP source, the first element of the instantaneous output Stokes vector is:

$$I_{outL}(t) = \rho I_0 \left[1 + d\sin(2\phi)\cos(\Delta\omega t)\right], \tag{24}$$

where the subscript L indicates the use of linear illumination states. This equation shows the essential characteristic of the orthogonality breaking sensing principle, namely an AC component in the output intensity which is due to the interference of the two SOP's, partially projected onto each other by the interaction with the diattenuator. Provided that the source can be tuned to set the frequency difference to a value that lies within the bandwidth of commercially-available detectors, it is then perfectly possible to observe the intensity beatnote with a fast photodiode.

According to the previous equation, the DC and AC components of the output intensity are respectively:

$$I^0_{outL} = \rho I_0, \tag{25}$$

$$I^{\Delta\omega X}_{outL} = \rho I_0 d\sin(2\phi), \tag{26}$$

the superscript ^{X} accounting for the in-phase component of the beatnote signal at $\Delta\omega$.

The Orthogonality Breaking Contrast (OBC) is a scalar parameter defined from the DC and AC components of the detected signal as:

$$\mathrm{OBC} = \frac{\overline{I^{\Delta\omega}_{out}}}{I^0_{out}}, \tag{27}$$

where $\overline{I^{\Delta\omega}_{out}} = \sqrt{\left(I^{\Delta\omega X}_{out}\right)^2 + \left(I^{\Delta\omega Y}_{out}\right)^2}$ is the amplitude of the detected beatnote signal. In this case, the quadrature component $I^{\Delta\omega Y}_{outL}$ is null, so $\overline{I^{\Delta\omega}_{outL}} = |I^{\Delta\omega X}_{outL}|$ and the OBC is thus:

$$\mathrm{OBC}_L = d|\sin(2\phi)|. \tag{28}$$

Concerning the phase of the AC signal, in this case it is obviously zero as $\angle I^{\Delta\omega}_{outL} = \arctan\left(I^{\Delta\omega Y}_{outL}/I^{\Delta\omega X}_{outL}\right)$. Consequently, when a linear DFDP source is used, the beatnote component does not undergo any phase delay while interacting with the dichroic sample, and the beatnote intensity depends on both the diattenuation coefficient d and the linear dichroism angle ϕ. It can be observed that the OBC takes a maximum value of d for a linear diattenuator oriented at $\phi = 45°$. This property has been used in previous works to calibrate the measurement system [27, 28].

If a circular DFDP source is now considered, the different components of the output intensity are:

$$I^0_{outC} = \rho I_0, \tag{29}$$

$$I^{\Delta\omega X}_{outC} = \rho I_0 d\sin(2\phi), \tag{30}$$

$$I^{\Delta\omega Y}_{outC} = -\rho I_0 d\cos(2\phi), \tag{31}$$

where the subscript C denotes circular illumination states. In this case the OBC and the beatnote signal phase are respectively:

$$\mathrm{OBC}_C = d, \tag{32}$$

$$\angle I^{\Delta\omega}_{outC} = 2\phi - \pi/2. \tag{33}$$

From the latter equation, the linear dichroism orientation can be readily obtained by:

$$\phi = \frac{1}{2}\left(\angle I^{\Delta\omega}_{outC} + \pi/2\right). \tag{34}$$

As a result, under circular illumination, the amplitude of the beatnote signal is independent of the dichroism orientation, giving access directly and without ambiguity to the sample dichroism. Moreover, the linear dichroism angle can be directly retrieved by the phase measurement. Such a feature is actually quite advantageous for linear dichroism sensing, as has been recently demonstrated in a microscopic imaging set-up [29].

4.D.2. Elliptical/circular diattenuator

The complete equations of the detected intensity when the sample presents elliptical dichroism are included in Appendix C. For the sake of conciseness, we shall only consider here the very specific case of a circular diattenuator whose Mueller matrix is:

$$\mathbf{M_{CD}} = \rho \begin{bmatrix} 1 & 0 & 0 & d \\ 0 & T & 0 & 0 \\ 0 & 0 & T & 0 \\ d & 0 & 0 & 1 \end{bmatrix}, \tag{35}$$

which is obtained by setting $\epsilon = \pi/4$ in the Mueller matrix of an elliptical diattenuator (Appendix A), T and d still corresponding to their initial definition given after Eq. (23). If the sample is illuminated with a linear DFDP source, the resulting OBC and phase are:

$$\mathrm{OBC}_L = d, \tag{36}$$

$$\angle I^{\Delta\omega}_{outL} = \pi/2. \tag{37}$$

These equations show that such a configuration is actually sensitive to circular dichroism, which is directly

characterized by the OBC, while the phase of the beatnote signal is constant. This latter information actually provides additional information about the dichroism properties when a linear DFDP source is used, as it is 0 for linear dichroism, $\pi/2$ for circular dichroism, and takes intermediate values for elliptical dichroism.

However, if a circular DFDP source is used, the OBC completely vanishes:

$$\mathrm{OBC}_C = 0, \tag{38}$$

which means that such a sample does not break the orthogonality between the circular SOP's. This is due to the fact that they are precisely the eigenstates of a circular diattenuator. Consequently, there is no beatnote signal in this case.

5. Orthogonality breaking sensing through a waveguide

In this section, orthogonality breaking sensing through a waveguide is considered. It is thus assumed that the source beam is delivered through a waveguide with Mueller matrix $\mathbf{M_{wg1}}$, when it impinges on the sample still described by its Mueller matrix $\mathbf{M}$, and is finally collected by a second waveguide with Mueller matrix $\mathbf{M_{wg2}}$ (which is not necessarily the same as the illumination one for the sake of generality), so the output instantaneous Stokes vector is:

$$\vec{\mathbf{S}}_{\mathbf{out}}(t) = \mathbf{M_{wg2}}\mathbf{M}\mathbf{M_{wg1}}\vec{\mathbf{S}}_{\mathbf{in}}(t). \tag{39}$$

We define the intermediate Stokes vector $\vec{\mathbf{S}}_{\mathbf{out'}}(t) = \mathbf{M}\mathbf{M_{wg1}}\vec{\mathbf{S}}_{\mathbf{in}}(t)$ as the instantaneous Stokes vector after interaction of the fiber-guided DFDP beam with the sample. In general, it can be assumed that an optical waveguide behaves as a retarder [25] (with possible isotropic loss, but with no dichroic effects). We thus model it by the Mueller matrix of a birefringent element. If we denote $I_{out'}$ the first element of the intermediate Stokes vector, one can readily verify that $I_{out} = I_{out'}$, as the Mueller matrix of a unitary optical element does not modify the beam intensity. A remarkable implication of this fact is that the collecting fiber does not modify the beatnote signal possibly produced by the sample, because such an information is exclusively carried by the intensity. This means that we can focus our analysis on the effect of the illuminating waveguide, while light collection can be performed by any non-dichroic optical waveguide.

Concerning the illuminating fiber, its effect is a modification of the orthogonal SOP's provided by the source, so it obviously has to be taken into account. The results for isotropic absorbers, elliptical retarders, and diagonal depolarizers are not discussed in this section, as the conclusions obtained in the previous section are valid regardless the SOP's of the DFDP illuminating beam. Moreover, if we focus on biomedical applications, circular dichroism is extremely unusual in biological samples [6, 35], so we will exclusively analyze fiber-guided orthogonality breaking sensing of linearly dichroic samples.

5.A. Waveguide acting as a circular retarder

Let us first consider a waveguide acting as a circular retarder, whose Mueller matrix is:

$$\mathbf{M_{CR}} = \begin{bmatrix} 1 & 0 & 0 & 0 \\ 0 & \cos(2\theta) & \sin(2\theta) & 0 \\ 0 & -\sin(2\theta) & \cos(2\theta) & 0 \\ 0 & 0 & 0 & 1 \end{bmatrix}, \tag{40}$$

θ being the optical rotation angle. If such a waveguide is used to illuminate a linear diattenuator with a DFDP source, it is easily shown that the results obtained in the previous section hold, up to a rotation angle of value θ due to optical rotation in the waveguide. Typically, one has $\mathrm{OBC}_L = d|\sin(2(\phi+\theta))|$ with a linear DFDP source, whereas $\mathrm{OBC}_C = d$ and $\angle I_{outC}^{\Delta\omega} = 2(\phi+\theta) - \pi/2$ with a circular DFDP source.

From these results, it is interesting to note that with circular DFDP illumination states, the presence of an illuminating waveguide acting as a rotator does not prevent from measuring the diattenuation coefficient, while the phase can be determined up to an additive term depending on the fiber.

5.B. Waveguide acting as a linear retarder

More typically, an optical waveguide behaves as a linear retarder, whose general Mueller matrix is:

$$\mathbf{M_{LR}} = \begin{bmatrix} 1 & 0 & 0 & 0 \\ 0 & \cos\delta\sin^2(2\psi) + \cos^2(2\psi) & (1-\cos\delta)\cos(2\psi)\sin(2\psi) & -\sin\delta\sin(2\psi) \\ 0 & (1-\cos\delta)\cos(2\psi)\sin(2\psi) & \cos\delta\cos^2(2\psi) + \sin^2(2\psi) & \sin\delta\cos(2\psi) \\ 0 & \sin\delta\sin(2\psi) & -\sin\delta\cos(2\psi) & \cos\delta \end{bmatrix}, \tag{41}$$

with ψ denoting the linear birefringence orientation, whereas δ stands for the retardation introduced between the birefringence slow and fast axes [32].

Illuminating a linear diattenuator through a linearly birefringent waveguide gives a lengthy expression of the

output intensity, that can be simplified to:

$$I^0_{outL} = \rho I_0, \tag{42}$$

$$I^{\Delta\omega X}_{outL} = I_0 \rho d \Big[\sin(2\psi)\cos(2(\phi-\psi)) + \cos(2\psi)\sin(2(\phi-\psi))\cos\delta \Big], \tag{43}$$

$$I^{\Delta\omega Y}_{outL} = I_0 \rho d \sin(\delta)\sin(2(\phi-\psi)). \tag{44}$$

It can be checked that when the linear birefringence axis of the waveguide is parallel to the linear dichroism ($\psi = \phi$), the previous equations are exactly the same as the results obtained without the waveguide (Eqs. (25-26)), i.e., $I^{\Delta\omega}_{outL,\delta\neq 0}(t) - I^{\Delta\omega}_{outL,\delta=0}(t) = 0$. However, in general the linear birefringence introduced by the waveguide can modify the calculated parameters, and produces an intrincate expression of the OBC. Let us define the bias of the measurement as

$$\mathrm{B}_L(t) = \frac{I^{\Delta\omega}_{outL,\delta\neq 0}(t) - I^{\Delta\omega}_{outL,\delta=0}(t)}{I^0_{outL}}. \tag{45}$$

With a linear DFDP source, the bias due to a linear birefringent waveguide then reads

$$\mathrm{B}_L(t) = 2d\sin\left(\frac{\delta}{2}\right)\left[-\cos(2\psi)\sin\left(\frac{\delta}{2}\right)\cos(\Delta\omega t) + \cos\left(\frac{\delta}{2}\right)\sin(\Delta\omega t)\right]\sin(2(\phi-\psi)). \tag{46}$$

If we consider the particular case of a slightly birefringent fiber ($\delta \ll 1$), the series expansion of $\mathrm{B}_L(t)$ in δ leads at first order in δ to

$$\mathrm{B}_L(t) = d\sin(2(\phi-\psi))\sin(\Delta\omega t)\delta + O(\delta). \tag{47}$$

If a circular DFDP source is now taken into account, the output intensity components are:

$$I^0_{outC} = \rho I_0, \tag{48}$$

$$I^{\Delta\omega X}_{outC} = I^{\Delta\omega X}_{outL} \tag{49}$$

$$I^{\Delta\omega Y}_{outC} = -I_0 \rho d \Big[\cos(2\psi)\cos(2(\phi-\psi)) - \sin(2\psi)\sin(2(\phi-\psi))\cos\delta \Big]. \tag{50}$$

Again, it can be verified that these equations coincide with the free-space sensing ones for the particular case in which the fiber optical axis is parallel to the sample linear dichroism ($\psi = \phi$). Nonetheless, any other situation leads to a modification of the results by the retarding action of the waveguide. Applying the bias defined in Eq. (45) to the circular DFDP source using Eqs. (49) and (50), one gets

$$\mathrm{B}_C(t) = 2d\sin\left(\frac{\delta}{2}\right)^2 \sin(2(\phi-\psi))\cos(\Delta\omega t - 2\psi). \tag{51}$$

If a slighly birefringent fiber is again considered, it can be verified that the bias is null at first order in δ, and that

$$\mathrm{B}_C(t) = d\sin(2(\phi-\psi))\cos(\Delta\omega t - 2\psi)\frac{\delta^2}{2} + O(\delta^2). \tag{52}$$

The bias in this case is actually at order 2 in δ. This is an interesting result, showing that the circular DFDP source is more advantageous for orthogonality breaking sensing through a linear birefringent waveguide, since the measured OBC is less prone to be biased by a slight birefringence in the waveguide.

6. Discussion

In this last section, we complement the preceding description of the orthogonality breaking signatures on various optically anisotropic samples by a discussion on the ability of this technique to sense depolarization. Indeed, even though calculations using the instantaneous Mueller-Stokes formalism in Section 4 show that the technique yields no orthogonality breaking contrast on a diagonal depolarizer, previous experimental results [27] seem to be in contradiction with this statement.

In order to clarify this essential aspect, we first performed a verification measurement using a linear DFDP blue source at $\lambda = 488$ nm whose development was detailed in a previous work [28]. The measurements were performed in free-space for two different diffusing samples, namely a blue paper and a red paper. The detector was fixed in a reflection configuration, with an incidence angle of roughly 45° on the sample. This measurement configuration was kept identical for both samples. As explained in detail in a previous work dealing with spectropolarimetric imaging of diffuse objects [36], illuminating both samples with a visible blue source yields two different situations. On the one hand, the main contribution to the backscattered light when the blue paper is measured comes from volume multiple scattering, as the incoming light is weakly absorbed. This type of scattering is very depolarizing, and its Mueller matrix corresponds to a diagonal depolarizer. On the other hand, when the red paper is used as a sample, the incident blue light beam is strongly absorbed by the red pigments. Consequently, the fraction of light reflected towards the detector mostly results from surface scattering, which implies much weaker depolarization and possible anisotropy of the reflection coefficients.

The measurements are presented in Fig. 2, which shows the AC component of the detected intensity for both samples using the linear DFDP source with the states oriented in two different ways, namely along the $0° - 90°$ and the $\pm 45°$ directions. In the first configuration, the two linear states of the DFDP beam respectively correspond to the so-called s and p polarization components at the surface, whereas in the second configuration both linear states have partial projections on the s and p directions. It can be observed that the AC component for the blue paper is almost zero regardless of the linear states orientation (dotted light blue curve and

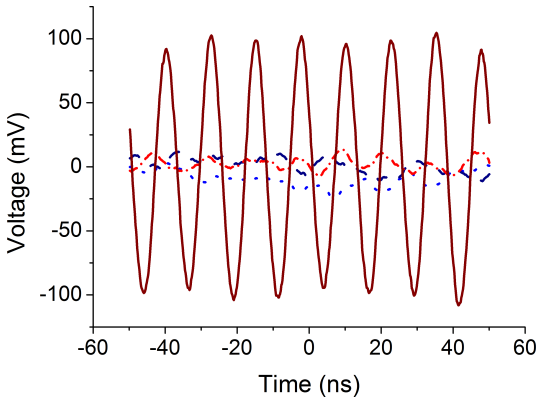

Fig. 2. AC component of the detected backscattered light under blue illumination for a blue paper and linear modes along the $0°-90°$ directions (dotted light blue curve) and the $\pm 45°$ directions (dashed dark blue curve), and for a red paper along the same directions (dashed-dotted light red curve and solid dark red curve respectively).

dashed dark blue curve respectively). In this case, the dominant effect is volume multiple scattering as mentioned above, which constitutes an initial verification of the fact that diagonal depolarization due to the sample does not produce an orthogonality breaking signal. Regarding the red paper, one can note that there is a slight variation from roughly no AC signal when the linear modes are oriented at $0° - 90°$ (dashed-dotted light red curve), to a substantial AC component when the modes are along $\pm 45°$ (solid dark red curve). This result is in agreement with the expected behaviour, as in this case surface effects are not masked by volume scattering, and thus slight differences in the reflectance coefficients for the s and p components of the incident light beam can result in dichroic effects in the polarized fraction of the detected backscattered light.

An appropriate interpretation of the aforementioned discrepancy between these results and some of our previous ones requires a deeper insight into the physical origins of depolarization. In the most general case, this generic notion must obviously encompass (i) the optical anisotropic properties of the sample considered; but also (ii) its local structural organization, including spatial randomization effects; (iii) the properties of the illumination field (e.g. spectral bandwidth); and (iv) the characteristics of the detection setup (e.g. numerical aperture [37] and spatial/spectral resolution). Describing a depolarizing medium with the Mueller matrix of a diagonal depolarizer (as $\mathbf{M_{\Delta}}$ in Eq. (22)) implicitly assumes full incoherent averaging over at least one of the above aspects. However, in a broad range of experimental setups the characteristics of the sensing/imaging system only lead to a partial averaging operation. As a result, the description of the sample by a diagonal depolarizing Mueller matrix is no longer physically appropriate in such cases.

In the remainder of this section, we propose to use a simple stochastic model of the Mueller matrix of a depolarizing anisotropic medium consisting of the action of random linear dichroic elements. It must be noted that this description does not represent a fully comprehensive model of depolarization, as many physical parameters involved in light depolarization are neglected. However, it is shown that it succesfully allows us to characterize the progressive transition from a deterministic anisotropic sample to a strongly random one (characterized by a Mueller matrix of a diagonal depolarizer) as the averaging conditions evolve. We then analyze the polarimetric properties of the resulting "macroscopic" depolarizing Mueller matrix obtained, and we characterize the orthogonality breaking signatures produced by such a sample and physical sensing conditions. A simple experimental validation using a synthetic depolarizing sample is also included. These results and discussions finally allow us to validate the calculations presented in this work, and to understand how the subtle aspects discussed regarding the measurement conditions were actually involved in our previous experimental measurements.

6.A. Stochastic depolarization model of an ensemble of random linear diattenuators

We consider the specific case of a dichroic depolarizing medium in which depolarization is due to the heterogeneity of its anisotropy properties. For that purpose, we consider that the incoming beam urdergoes random local dichroic interactions, each polarization transformation having a diattenuation coefficient d_μ, linear dichroism angle ϕ_μ, isotropic absorption ρ_μ, and transmission parameter T_μ, where μ denotes one realization of a random event. The effect of a given random event on a DFDP illumination beam is obviously strictly equivalent to the one studied in Section 4, and can consequently be represented by a single Mueller matrix $\mathbf{M_{LD}}_\mu$ with the same form as that given in Eq. (23). Consequently, the Mueller matrix of a single random event is not depolarizing (Mueller-Jones matrix), as the individual polarization transformation is purely deterministic. In this case, there is a well-known one-to-one relationship between $\mathbf{M_{LD}}_\mu$ and its corresponding Jones matrix, as stated in Eq. (A-3) of Appendix A [38, 39].

The macroscopic Mueller matrix of the sample that determines the detected intensity now implies averaging over random events, i.e., $\mathbf{M^{\Delta}_{LD}} = \langle \mathbf{M_{LD}}_\mu \rangle_\mu$. For the sake of simplicity, let us assume that the random variable ϕ_μ is independent from d_μ and ρ_μ. Regarding its probability density function, we propose to adopt a convenient statistical model for angular random variables, namely the Wrapped-Gaussian Distribution (WGD), with average value $\bar{\phi}$ and variance σ^2_ϕ [40]. The definition and main properties of WGD's, which basically correspond to normal probability distributions 'wrapped' around the unit circle, are recalled in Appendix D. Using these properties, the ensemble-averaged Mueller matrix of the

sample is:

$$\mathbf{M}^{\mathbf{\Delta}}_{\mathbf{LD}} = \langle \mathbf{M}_{\mathbf{LD}\mu} \rangle_\mu = \bar{\rho} \begin{bmatrix} 1 & \bar{d}\cos 2\bar{\phi}\, e^{-2\sigma_\phi^2} & \bar{d}\sin 2\bar{\phi}\, e^{-2\sigma_\phi^2} & 0 \\ \bar{d}\cos 2\bar{\phi}\, e^{-2\sigma_\phi^2} & \frac{1+\langle T\rangle}{2} + \frac{1-\langle T\rangle}{2}\cos 4\bar{\phi}\, e^{-8\sigma_\phi^2} & (1-\langle T\rangle)\cos 2\bar{\phi}\sin 2\bar{\phi}\, e^{-8\sigma_\phi^2} & 0 \\ \bar{d}\sin 2\bar{\phi}\, e^{-2\sigma_\phi^2} & (1-\langle T\rangle)\cos 2\bar{\phi}\sin 2\bar{\phi}\, e^{-8\sigma_\phi^2} & \frac{1+\langle T\rangle}{2} - \frac{1-\langle T\rangle}{2}\cos 4\bar{\phi}\, e^{-8\sigma_\phi^2} & 0 \\ 0 & 0 & 0 & \langle T\rangle \end{bmatrix}, \tag{53}$$

where, for the sake of generality, random variables T_{min} and T_{max} are simply assumed to admit average values $\overline{T}_{min}$ and $\overline{T}_{max}$, hence $\bar{\rho} = (\overline{T}_{max} + \overline{T}_{min})/2$, and we set $\bar{d} = (\overline{T}_{max} - \overline{T}_{min})/2\bar{\rho}$.

From this matrix, the output intensity can be obtained from Eq. (19) (in the same way as the calculations detailed in Sections 4 and 5), and it is quite straightforwardly shown that the orthogonality breaking contrast obtained for this sample is

$$\mathrm{OBC}_L = \bar{d}e^{-2\sigma_\phi^2}|\sin 2\bar{\phi}| \tag{54}$$

in the case of linear input polarization states, whereas circular states would yield

$$\mathrm{OBC}_C = \bar{d}e^{-2\sigma_\phi^2}, \quad \text{and} \quad \angle I^{\Delta\omega}_{outC} = 2\bar{\phi} - \frac{\pi}{2}. \tag{55}$$

These results are very similar to the case of deterministic transformations of the state of polarization (Eq. (28) and Eqs. (32) and (33)), up to a "fading" factor of the beatnote amplitude equal to $e^{-2\sigma_\phi^2}$. As a result, a strong dispersion of the dichroism orientations would blur the orthogonality breaking signal produced by the diattenuation properties of the sample. Once again, one can note that using circular input states is more favourable, since the mean value of the diattenuation orientation $\bar{\phi}$ can be retrieved from the measurement of the beatnote phase, provided the beatnote amplitude is not completely attenuated.

To further analyze the previous results, let us now assume that the diattenuation angle ϕ_μ is the only random parameter, d, ρ and T being now considered as deterministic. On the one hand, it can be immediately observed that when $\sigma_\phi \to 0$, $\mathbf{M}^{\mathbf{\Delta}}_{\mathbf{LD}\sigma_\phi\to 0} = \mathbf{M_{LD}}$, which corresponds to the trivial case of a deterministic sample, whose measurement using the orthogonality breaking technique obviously yields the same results as those obtained in the previous sections. On the other hand, when the angular distribution becomes strongly randomized (i.e., $\sigma_\phi \gg 1$), the Mueller matrix tends to the form of a diagonal depolarizer:

$$\mathbf{M}^{\mathbf{\Delta}}_{\mathbf{LD}\sigma_\phi\gg 1} = \rho\ \mathrm{diag}\big[1,\ (1+T)/2,\ (1+T)/2,\ T\big]. \tag{56}$$

We recall that if dichroism is perfect ($d = 1$), then $T = 0$ and the previous matrix corresponds to a sample that completely depolarizes the fourth element of the Stokes vector, and reduces by 0.5 the DOP of any linear input SOP. For other values of T, the depolarization strength of such a diagonal depolarizer for each Stokes vector element varies. In any case, it is verified that the resulting intensity is constant $I_{out}(t) = \rho I_0$ (in agreement with the results obtained in Section 4.C for diagonal depolarizers), so no orthogonality breaking signal appears. Apart from that, we note that $\mathbf{M}^{\mathbf{\Delta}}_{\mathbf{LD}\sigma_\phi\gg 1}$ turns out to be proportional to the identity matrix (isotropic absorption) when $T \to 1$ (or equivalently $d \to 0$). These features confirm that the presented approach makes it possible to simply model the continuous transition from a non-depolarizing sample characterized by a deterministic polarization transformation on the one hand, to a fully depolarizing sample depending on the statistical properties of the random diattenuation parameters on the other hand.

The polarimetric properties of the stochastic Mueller matrix obtained above can now be quantified by several parameters. The first one is the diattenuation coefficient, that can be calculated from $\mathbf{M}^{\mathbf{\Delta}}_{\mathbf{LD}}$ (assuming again that ϕ_μ is the only random parameter) by [33]

$$D = \frac{\sqrt{\sum_{j=2}^{4}(\mathbf{M}^{\mathbf{\Delta}}_{\mathbf{LD}})^2_{1j}}}{(\mathbf{M}^{\mathbf{\Delta}}_{\mathbf{LD}})_{11}} = de^{-2\sigma_\phi^2}, \tag{57}$$

showing that it scales exactly as the OBC with the angular dispersion. As a result, on this sample, the orthogonality breaking technique using circular states for instance would provide a direct measure of the *effective* linear diattenuation of the sample (as $\mathrm{OBC}_C = D = de^{-2\sigma_\phi^2}$), and of the average diattenuation orientation $\bar{\phi}$. The evolution of the effective dichroism D is plotted in Fig. 3.(a) as a function of σ_ϕ and of $\log_{10} T_{max}/T_{min}$ (which is 0 for an isotropic sample and tends to infinity for a perfect polarizer). It can be seen that the effective linear dichroism rapidly decreases with σ_ϕ, whereas it increases for higher $\log_{10} T_{max}/T_{min}$ as expected. The evolution of D for $\sigma_\phi = 0$ corresponds to the diattenuation coefficient of a linear diattenuator with a fixed deterministic orientation.

It is now interesting to analyze the depolarizing properties of the $\mathbf{M}^{\mathbf{\Delta}}_{\mathbf{LD}}$ matrix. There are several depolarization metrics that can be used to quantify the depolarizing properties of a sample [33, 41–45]. In this work we use the Cloude entropy, which is a well-established metric to characterize the overall depolarizing nature

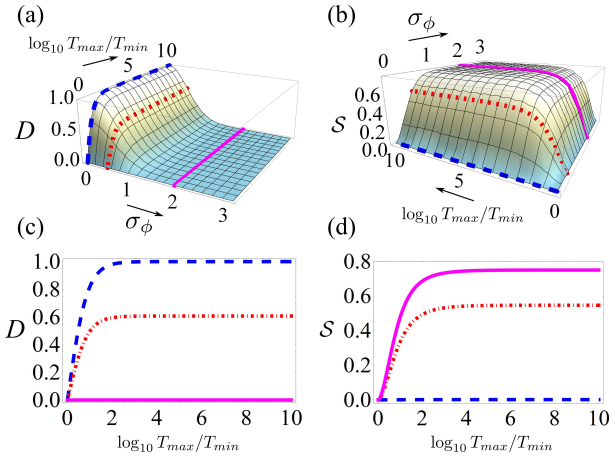

Fig. 3. (a) Evolution of the effective diattenuation coefficient D as a function of angular dispersion σ_ϕ and of $\log_{10} T_{max}/T_{min}$. (b) Evolution of the Cloude entropy $\mathcal{S}$ as a function of angular dispersion σ_ϕ and of $\log_{10} T_{max}/T_{min}$. Evolution of the diattenuation coefficient D (c) and of the Cloude entropy $\mathcal{S}$ (d) as a function of $\log_{10} T_{max}/T_{min}$ for $\sigma_\phi = 0$ (blue), $\sigma_\phi = 1/2$ (red), and $\sigma_\phi = 2$ (magenta).

of a given Mueller matrix [41]. The Cloude entropy is given by $\mathcal{S} = -\sum_{i=1}^{4} \lambda'_i \log_4 \lambda'_i$, where $\lambda'_i = \lambda_i / \sum_{j=1}^{4} \lambda_j$ are the normalized eigenvalues of the 4×4 Cloude coherency matrix [41], whose derivation from $\mathbf{M}^{\mathbf{\Delta}}_{\mathbf{LD}}$ is detailed in Appendix E. The Cloude entropy $\mathcal{S}$ is plotted in Fig. 3.(b) as a function of σ_ϕ and of $\log_{10} T_{max}/T_{min}$. To facilitate the physical interpretation, the evolution of parameters D and $\mathcal{S}$ with $\log_{10} T_{max}/T_{min}$ for three different values of σ_ϕ (namely 0, 1/2 and 2) are respectively plotted in Figs. 3.(c) and (d).

It can be seen in Fig. 3.(b) that the Cloude entropy $\mathcal{S}$ increases with σ_ϕ, thus evidencing that depolarization is stronger as the angular dispersion grows. On the other hand, the Cloude entropy increases with $\log_{10} T_{max}/T_{min}$. The Mueller matrix of the sample at $\sigma_\phi = 0$ or $\log_{10} T_{max}/T_{min} = 0$ corresponds to a deterministic Mueller matrix, hence leading to a null entropy. The Cloude entropy reaches a maximum at $\mathcal{S} = 0.75$ for high values of σ_ϕ and significant anisotropy ($\log_{10} T_{max}/T_{min} \neq 0$). It can be noted that the maximum Cloude entropy does not reach unity, simply because the stochastic model of the sample considered does not lead to a complete depolarization of any input SOP, as we have only considered the subset of random linearly dichroic events without including elliptical dichroism.

More generally, the joint analysis of the plots in Fig. 3.(a) and 3.(b) clearly confirms the gradual evolution of $\mathbf{M}^{\mathbf{\Delta}}_{\mathbf{LD}}$ from a deterministic Mueller matrix of a diattenuator ($\mathcal{S} = 0$, $D \neq 0$) to a depolarizing Mueller matrix (maximum $\mathcal{S}$, $D \to 0$) when the angular dispersion σ_ϕ increases, as predicted by Eq. (53). In other words, we observe that the intrinsic dichroic properties of the sample gradually vanishe as more orientations of the dichroism are taken into account by increasing σ_ϕ, providing the sample with a "macroscopic" depolarizing nature.

6.B. Interpretation of experimental results

The previous results can be easily confirmed on a simple laboratory experiment. For that purpose, we used the DFDP visible source ($\lambda = 488$ nm) emitting linear polarization states to shine a sample composed of two orthogonally-oriented linear polaroid sheets placed in juxtaposition to each other. A sketch of the sample is presented in the inset of Fig. 4. The position of the laser beam is then displaced along the sample, whose Mueller matrix $\mathbf{M_s}$ can be written

$$\mathbf{M_s} = A\ \mathbf{M}_{\mathbf{LD}_{\phi=0}} + (1-A)\mathbf{M}_{\mathbf{LD}_{\phi=\pi/2}}, \qquad (58)$$

where A is the fraction of the laser spot area lying on the horizontal polarizer. In the central position $A = 1/2$, so both polarizers equally contribute to the detected intensity, and the resulting Mueller matrix is:

$$\mathbf{M}_{\mathbf{s}_{center}} = \rho\ \mathrm{diag}\big[1,\ 1,\ T,\ T\big]. \qquad (59)$$

It is readily observed that such a Mueller matrix corresponds to a diagonal depolarizer. The commercial polaroid sheets used satisfy $T \simeq 0$, so when the laser spot is centered in the middle of the synthetic sample proposed in this section (i.e., $x_b = 0$), it behaves as a diagonal depolarizer that completely depolarizes the third and fourth elements of the input Stokes vector, without altering the second one appart from the isotropic absorption. As a result, such a sample provides an OBC that evolves from a maximum value when the spot entirely lies on a single polaroid sheet, to a null value when it is placed at the center. The same conclusion can be reached by separately calculating the output intensities for $\phi = 0$ and $\phi = \pi/2$ using Eq. (26) and adding them, which results in a destructive interference between both beatnote signals in the central position since they show a relative phase of π.

The OBC for this sample was measured using the previously reported setup in transmission [29]. The evolution of the OBC as a function of the beam position is plotted in Fig. 4. This experimental curve follows the expected behaviour, evidencing how the maximum orthogonality breaking contrast obtained on a perfectly dichroic sample (extremal positions of the sample) is gradually lost as the beam simultaneously interacts with two orthogonally-oriented polarizers. Indeed, it is confirmed that when the beam is centered, both contributions from each half of the beam destructively interfere on the detector, resulting in a null beatnote amplitude.

In light of all the above results, we are now able to provide an interpretation of the discrepancy between the theoretical predictions presented in Section 4 and the experimental observations at $\lambda = 1.55$ μm reported in [27]. In that work, orthogonality breaking measurements were carried out in a fibered configuration, and then compared to the control values determined with a standard

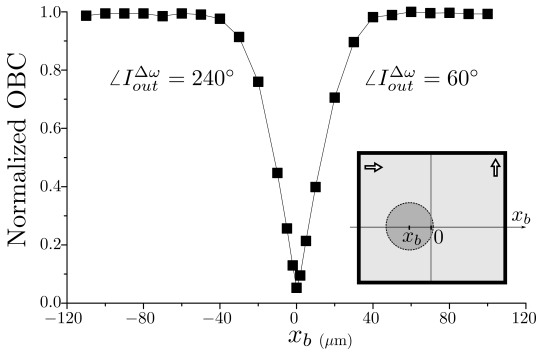

Fig. 4. Evolution of the OBC and phase as a function of beam position. Inset: sketch of the synthetic sample composed of a juxtaposition of two orthogonally oriented polarizing sheets. The illumination beam centered in x_b is made to horizontally scan across the sample, $x_b = 0$ corresponding to the juxtaposition edge of the two polarizing sheets.

free-space Stokes polarimeter at $\lambda = 1.55$ μm. According to the discussions presented in this section, the difference in the experimental conditions of both measurements can have strong consequences on the measured depolarization. Indeed, the standard Stokes polarimetry measurements were carried out in free-space, with a relatively high spot size on the sample and high numerical aperture for the light collection. Such an experimental configuration effectively implies a spatial averaging operation over the sample surface and over several spatial coherence areas (speckle grains) as discussed in [37]. However, the OB signals detected on the same samples were collected through a standard single-mode SMF28 optical fiber whose FC-APC connector end was placed in vicinity of the samples. Under such conditions, the spatial or angular averaging is very moderate, which presumably corresponds to an intermediate position in the aforementioned transition from a non-depolarizing sample to a depolarizing one. In that case, both the diattenuation coefficient and the sample depolarization lie between their respective maximum and minimum values, as shown in Fig. 3. Therefore, in light of the thorough modelization proposed in this work and of the discussion detailed in this section, we can conclude that the OBC measured in [27] were most likely due to a moderate spatial averaging of the local diattenuation properties of the samples rather than pure depolarization.

7. Conclusion

In this work, the instantaneous Stokes-Mueller formalism has been applied to conveniently describe the DFDP beam used in the polarimetric sensing by orthogonality breaking technique, and to model the interaction of such a beam with anisotropic depolarizing media. Based on this formalism, we have thoroughly analyzed the characteristics of the orthogonality breaking signal after interacting with birefringent, dichroic, and depolarizing samples. It has thus be confirmed that this measurement technique provides a direct characterization of dichroic samples, and that using a circular DFDP source makes it possible to readily determine the diattenuation magnitude and orientation from the amplitude and the phase of the detected intensity. Moreover, the insensitivity of this technique to birefringence has been confirmed both theoretically and experimentally. This constitutes an interesting property for remote polarimetric measurements, especially for endoscopic applications involving optical fibers. We have consequently characterized the influence of a birefringent waveguide on the detected beatnote component, showing that the orthogonality breaking contrast is affected by a slight bias at order two in the residual fiber birefringence when a circular DFDP source is used.

Lastly, we have proposed a simple stochastic model of a depolarizing sample composed of randomly-oriented linear diattenuators. Such an analytical model, along with the results of a simple and meaningful laboratory experiment, clearly illustrates the gradual orthogonality breaking contrast vanishing as the orientation randomization of the sample increases, due to the destructive interference of the dephased individual orthogonality breaking beatnotes. All these considerations have led us to reinterpret our first experimental results, in which the observed orthogonality breaking contrast was most likely due to the effective diattenuation of the samples rather than to their depolarizing properties. Consequently, in light of the comprehensive model and the experimental measurements presented in this work, it is concluded that the orthogonality breaking technique is insensitive to diagonal depolarization. This is an important property to be highlighted. Indeed, most polarimetric techniques are influenced by depolarization, which encompasses many physical aspects, including the structural properties of the sample, the detection geometry, and the source and detector bandwidth. Being exclusively sensitive to dichroism, the orthogonality breaking technique is thus remarkably advantageous for characterizing such a parameter without being affected by other sample properties, hence potentially leading to a more specific and robust sample characterization.

The general method presented in this work provides an in-depth analysis on the physical origin of the detected signals in different measurement configurations. These results allow orthogonality breaking sensing to be adequately modeled, which paves the way for the optimal design of orthogonality breaking imaging systems with the capacity to perform direct and fast polarimetric measurements at high dynamics. The future development of this technique includes a systematic comparative study with standard polarimetric imaging techniques in various application contexts, and its extension to remote endoscopic measurements through fiber bundles for biomedical applications.

Appendix A

A characteristic property of the Jones matrix of a general dichroic sample is that its two eigenvalues are real and take the form $\lambda_1 = T_{max}^{1/2}$ and $\lambda_2 = T_{min}^{1/2}$, where T_{max} and T_{min} are respectively the maximum and minimum transmittances. If we consider the eigenvector $\vec{\mathbf{E}}_{\mathbf{eig}}$ corresponding to the greatest eigenvalue:

$$\vec{\mathbf{E}}_{\mathbf{eig}} = \begin{bmatrix} a \\ b \end{bmatrix}, \tag{A-1}$$

the Jones matrix of any elliptic dichroic sample is, according to Ref. [46]:

$$\mathbf{J_{ED}} = \begin{bmatrix} \lambda_1 aa^* + \lambda_2 bb^* & (\lambda_1 - \lambda_2)\, ab^* \\ (\lambda_1 - \lambda_2)\, ba^* & \lambda_2 aa^* + \lambda_1 bb^* \end{bmatrix}. \tag{A-2}$$

If a and b are parameterized according to the general expressions given in Eq. (10), the Mueller matrix $\mathbf{M_{ED}}$ of an elliptical diattenuator can be readily obtained by applying the well-known relationship between a Jones matrix and its equivalent Mueller-Jones matrix:

$$\mathbf{M} = \mathbf{T}\big(\mathbf{J} \otimes \mathbf{J}^*\big)\mathbf{T}^{-1}, \tag{A-3}$$

where $\otimes$ stands for Kronecker product and matrix $\mathbf{T}$ is

$$\mathbf{T} = \begin{pmatrix} 1 & 0 & 0 & 1 \\ 1 & 0 & 0 & -1 \\ 0 & 1 & 1 & 0 \\ 0 & i & -i & 0 \end{pmatrix}, \tag{A-4}$$

which satisfies $\mathbf{T}^{-1} = 1/2\mathbf{T}^\dagger$ [39]. From the previous equations, the explicit form of $\mathbf{M_{ED}}$ is found to be:

$$\mathbf{M_{ED}} = \rho \begin{bmatrix} 1 & dC_{2\phi}C_{2\epsilon} & dS_{2\phi}C_{2\epsilon} & dS_{2\epsilon} \\ dC_{2\phi}C_{2\epsilon} & \frac{1+3T}{4} + \frac{1-T}{4}\big[C_{4\epsilon} + 2C_{4\phi}S_{2\epsilon}^2\big] & \frac{1-T}{2}S_{4\phi}C_{2\epsilon}^2 & \frac{1-T}{2}C_{2\phi}S_{4\epsilon} \\ dS_{2\phi}C_{2\epsilon} & \frac{1-T}{2}S_{4\phi}C_{2\epsilon}^2 & \frac{1+3T}{4} + \frac{1-T}{4}\big[C_{4\epsilon} - 2C_{4\phi}S_{2\epsilon}^2\big] & \frac{1-T}{2}S_{2\phi}S_{4\epsilon} \\ dS_{2\epsilon} & \frac{1-T}{2}C_{2\phi}S_{4\epsilon} & \frac{1-T}{2}S_{2\phi}S_{4\epsilon} & \frac{1+T}{2} - \frac{1-T}{2}C_{4\epsilon} \end{bmatrix}, \tag{A-5}$$

where the compact notation $C_{k\phi}^n = \cos^n(k\phi)$ and $S_{k\phi}^n = \sin^n(k\phi)$ has been used. The well-known matrix of an ideal elliptical diattenuator [38] results from substituting $T_{max} = 1$ and $T_{min} = 0$, so $\rho = 1/2$, $d = 1$ and $T = 0$ in the previous equation.

Appendix B

We shall consider a linear diattenuator illuminated by a non-balanced linear DFDP source, whose instantaneous Stokes vector is given in Eq. (13). The output intensity shows the following DC and in-phase AC components:

$$I_{outL}^0 = \rho I_0 + d\frac{1-\gamma}{1+\gamma}\cos(2\phi), \tag{B-1}$$

$$I_{outL}^{\Delta\omega X} = 2\rho I_0 \frac{\sqrt{\gamma}}{1+\gamma} d\sin(2\phi). \tag{B-2}$$

It can be shown that the calculation of the OBC parameter according to Eq. (27) does not provide useful information for characterizing the sample dichroism, as the sample parameters ρ, d, and ϕ are strongly mixed. If a non-balanced circular DFDP source is instead used, the DC, in-phase and quadrature components of the output intensity are:

$$I_{outC}^0 = \rho I_0, \qquad I_{outC}^{\Delta\omega X} = I_{outL}^{\Delta\omega X}, \tag{B-3}$$

$$I_{outC}^{\Delta\omega Y} = -2\rho I_0 d\frac{\sqrt{\gamma}}{1+\gamma}\cos(2\phi). \tag{B-4}$$

In this case, the OBC and the beatnote signal phase are respectively:

$$\mathrm{OBC}_C = 2d\frac{\sqrt{\gamma}}{1+\gamma}, \quad \text{and,} \quad \angle I_{outC}^{\Delta\omega} = 2\phi - \pi/2. \tag{B-5}$$

It should be noted that the OBC is directly the diattenuation coefficient if $\gamma = 1$. Therefore, a balanced source constitutes the most appropriate choice for our purposes. Regarding the phase of the beatnote signal, it enables the linear dichroism orientation to be readily obtained, as discussed in Section 4.

Appendix C

We shall now consider a sample with elliptic dichroism, whose Mueller matrix $\mathbf{M_{ED}}$ has been derived in Appendix A. Using a linear DFDP source, the output is:

$$I_{outL}^0 = \rho I_0, \tag{C-1}$$

$$I_{outL}^{\Delta\omega X} = \rho I_0 d\cos(2\epsilon)\sin(2\phi), \tag{C-2}$$

$$I_{outL}^{\Delta\omega Y} = \rho I_0 d\sin(2\epsilon), \tag{C-3}$$

which results in the following parameters:

$$\mathrm{OBC}_L = d\sqrt{\sin^2(2\epsilon) + \cos^2(2\epsilon)\sin^2(2\phi)}, \tag{C-4}$$

$$\angle I_{outL}^{\Delta\omega} = \arctan\left[\frac{\tan(2\epsilon)}{\sin(2\phi)}\right]. \tag{C-5}$$

Using a circular DFDP source, the results are:

$$I_{outC}^0 = \rho I_0, \quad I_{outC}^{\Delta\omega X} = I_{outL}^{\Delta\omega X}, \tag{C-6}$$

$$I_{outC}^{\Delta\omega Y} = -\rho I_0 d\cos(2\epsilon)\cos(2\phi), \tag{C-7}$$

which leads to:

$$\mathrm{OBC}_C = d|\cos(2\epsilon)|, \tag{C-8}$$

$$\angle I_{outC}^{\Delta\omega} = 2\phi - \pi/2. \tag{C-9}$$

We can highlight two aspects of this configuration. The first one is that the measured diattenuation coefficient d diminishes as a function of the dichroism ellipticity, completely vanishing in the case of circular dichroism. The second one is that the phase of the beatnote signal is the same regardless of the sample ellipticity, so it can be extracted in the same way as in Eq. (34).

Appendix D

Let θ be a random variable distributed according to a Wrapped-Gaussian distribution (WGD) with probability density function (pdf) [40]

$$f_{WG}(\theta;\mu,\sigma) = \frac{1}{\sqrt{2\pi}\sigma}\sum_{k=-\infty}^{+\infty} e^{-\frac{\left(\theta-\mu+2k\,\pi\right)^2}{2\sigma^2}}, \qquad \text{(D-1)}$$

where the parameters μ and σ respectively identify with the mean and standard deviation of θ. Such a WGD verifies the following property:

$$\langle z^n\rangle = \int_\Gamma e^{in\theta} f_{WG}(\theta;\mu,\sigma)d\theta = e^{in\mu}e^{-\frac{n^2\,\sigma^2}{2}}, \qquad \text{(D-2)}$$

where $z = e^{i\theta}$, and Γ is an integration interval of length 2π. As a result, the first moments of z are thus $\langle z\rangle = e^{i\mu}e^{-\frac{\sigma^2}{2}}$ and $\langle z^2\rangle = e^{2i\mu}e^{-2\sigma^2}$ and one has

$$\begin{aligned}\langle\sin\theta\rangle &= e^{-\frac{\sigma^2}{2}}\sin\mu,\\ \langle\cos\theta\rangle &= e^{-\frac{\sigma^2}{2}}\cos\mu.\end{aligned} \qquad \text{(D-3)}$$

Appendix E

The Cloude coherency matrix $\mathbf{CM}$ of a Mueller matrix $\mathbf{M}$ can be straightfully derived from the relations given in [41]: $\mathbf{CM} = (\sum_{j,k=1}^{4}\mathbf{M}_{jk}\;\boldsymbol{\eta}_{jk})/4$, with $\boldsymbol{\eta}_{jk} = \mathbf{T}\big(\sigma_j\otimes\sigma_k^*\big)\mathbf{T}^\dagger$, where the $\boldsymbol{\sigma}_{i,\,i\in[1,4]}$ stand for the standard Pauli matrices, and where $\mathbf{T}$ is given in Eq. (A-4). Using these relations, one obtains the Cloude coherency matrix of $\mathbf{M}^{\boldsymbol{\Delta}}_{\mathbf{LD}}$ (Eq. (53)), as

$$\mathbf{CM}^{\boldsymbol{\Delta}}_{\mathbf{LD}} = \rho\begin{bmatrix}\mathbf{CM}^{\boldsymbol{\Delta}}_{\mathbf{LD},\mathbf{3\times3}} & \vec{0}\\ \vec{0}^{\mathrm{T}} & 0\end{bmatrix}, \qquad \text{(E-1)}$$

where the upper 3×3 matrix $\mathbf{CM}^{\boldsymbol{\Delta}}_{\mathbf{LD},\mathbf{3\times3}}$ reads

$$\rho\begin{bmatrix}1{+}\langle T\rangle & \bar{d}\,C_{2\bar{\phi}}\,e^{-2\sigma_\phi^2} & \bar{d}\,S_{2\bar{\phi}}\,e^{-2\sigma_\phi^2}\\ \bar{d}\,C_{2\bar{\phi}}\,e^{-2\sigma_\phi^2} & \frac{1\text{-}\langle T\rangle}{2}\big[1{+}C_{4\bar{\phi}}\,e^{-8\sigma_\phi^2}\big] & \frac{1\text{-}\langle T\rangle}{2}S_{4\bar{\phi}}\,e^{-8\sigma_\phi^2}\\ \bar{d}\,S_{2\bar{\phi}}\,e^{-2\sigma_\phi^2} & \frac{1\text{-}\langle T\rangle}{2}S_{4\bar{\phi}}\,e^{-8\sigma_\phi^2} & \frac{1\text{-}\langle T\rangle}{2}\big[1\text{-}C_{4\bar{\phi}}\,e^{-8\sigma_\phi^2}\big]\end{bmatrix}. \qquad \text{(E-2)}$$

It can be clearly seen that this matrix is of rank three as soon as $\sigma_\phi \neq 0$, whereas it is of rank one (independently of σ_ϕ) when $\langle T\rangle = 1$ (isotropic case) thus leading to null Cloude entropy ($\mathcal{S} = 0$).

Acknowledgments

This work has been funded by the French National Defense Agency (DGA) and National Research Agency (ANR) project RADIO LIBRE (ANR-13-ASTR-0001) and by Région Bretagne.

References

[1] J. S. Tyo, D. L. Goldstein, D. B. Chenault and J. A. Shaw, "Review of passive imaging polarimetry for remote sensing applications," Appl. Opt. **45**, 5453–69 (2006).

[2] J. Tinbergen, *Astronomical polarimetry* (Cambridge University Press, 1996).

[3] F. Goudail, Ph. Réfrégier, "Target segmentation in active polarimetric images by use of statistical active contours," Appl. Opt. **41**, 874–83 (2002).

[4] S. G. Demos, and R. R. Alfano, "Optical fingerprinting using polarisation contrast improvement," Electronic Letters, **33**, 582–4 (1997).

[5] J. M. Bueno, J. J. Hunter, C. J. Cookson, M. L. Kisilak and M. C. W. Campbell, "Improved scanning laser fundus imaging using polarimetry," J. Opt. Soc. Am. A **24**, 1337–48 (2007).

[6] N. Ghosh and I. A. Vitkin, "Tissue polarimetry: concepts, challenges, applications, and outlook," J. Biomed. Opt. **16**, 110801 (2011).

[7] M. H. Smith, P. D. Burke, A. Lompado, E. A. Tanner, and L. W. Hillman, "Mueller matrix imaging polarimetry in dermatology," Proc. SPIE **3911**, 210–6 (2000).

[8] A. Pierangelo, A. Benali, M.-R. Antonelli, T. Novikova, P. Validire, B. Gayet, A. De Martino, "Ex-vivo characterization of human colon cancer by Mueller polarimetric imaging," Opt. Express **19**, 1582–93 (2011).

[9] J. S. Lee, M. R. Grunes, E. Pottier, "Quantitative comparison of classification capability: fully polarimetric versus dual and single-polarization SAR," IEEE Transactions on Geoscience and Remote Sensing **39**, 2343–51 (2001).

[10] F. Meriaudeau, M. Ferraton, C. Stolz, O. Morel, and L. Bigue, "Polarization imaging for industrial inspection," Proc. SPIE 6813, Image Processing: Machine vision applications, 681308 (2008).

[11] J. Fade, S. Panigrahi, A. Carré,1 L. Frein, C. Hamel, F. Bretenaker, H. Ramachandran, and M. Alouini, "Long-range polarimetric imaging through fog," Appl. Opt. **53**, 3854–65 (2014).

[12] J. S. Tyo , "Design of optimal polarimeters: maximization of signal-to-noise ratio and minimization of systematic error," Appl. Opt. **41**, 619–30 (2002).

[13] A .De Martino, Y.-K. Kim, E. García-Caurel, B. Laude, B. Drévillon, "Optimized Mueller polarimeter with liquid crystals," Opt. Lett **28**, 616–8 (2003).

[14] S. Jiao, M. Todorovic, G. Stoica, and L. V. Wang, "Fiber-based polarization-sensitive Mueller matrix optical coherence tomography with continuous source polarization modulation," Appl. Opt. **44**, 5463–7 (2005).

[15] C. F. LaCasse, R. A. Chipman, and J. S. Tyo, "Band limited data reconstruction in modulated polarimeters," Opt. Express **19**, 14976–89 (2011).

[16] A. S. Alenin and J. S. Tyo, "Generalized channeled polarimetry," J. Opt. Soc. Am. A **31**, 1013–22 (2014).

[17] A. Le Gratiet, S. Rivet, M. Dubreuil, and Y. Le Grand, "100 kHz Mueller polarimeter in reflection configuration," Opt. Lett. **40**, 645–8 (2015).

[18] G. Anna, H. Sauer, F. Goudail and D. Dolfi, "Fully tunable active polarization imager for contrast enhancement and partial polarimetry," Appl. Opt. **51**, 5302–9 (2012).

[19] T. T. Tower, and R. T. Tranquillo, "Alignment maps of tissues: II. Fast harmonic analysis for imaging," Bio-

physical Journal, **81**, 2964–71 (2001).
[20] Ph. Réfrégier, J. Fade and M. Roche, "Estimation precision of the degree of polarization from a single speckle intensity image," Opt. Letters **32**, 739–41 (2007).
[21] Z. Nan, J. Xiaoyu, H. Yonghong, and M. Hui, "Linear polarization difference imaging and its potential applications," Appl. Opt. **48**, 6734–9 (2009).
[22] T. C. Wood and D. S. Elson,"Polarization response measurement and simulation of rigid endoscopes," Biomed. Opt. Express **1**, 464–70 (2010).
[23] N. Thekkek, M. C. Pierce, M. H. Lee, A. D. Polydorides, R. M. Flores, S. Anandasabapathy and R. R. Richards-Kortum ,"Modular video endoscopy for in vivo cross-polarized and vital-dye fluorescence imaging of Barrett's-associated neoplasia," J. Biomed. Opt. **18**, 026007 (2013).
[24] J. Qi, M. Ye, M. Singh, NT. Clancy, and DS. Edson, "Narrow band 3×3 Mueller polarimetric endoscopy," Biomed. Opt. Express **4**, 2433–49 (2013).
[25] S. Manhas, J. Vizet, S. Deby, J.-C. Vanel, P. Boito, M. Verdier, A. De Martino, and D. Pagnoux, "Demonstration of full 4×4 Mueller polarimetry through an optical fiber for endoscopic applications," Opt. Express **23**, 3047–54 (2015).
[26] J. Vizet, J. Brevier, J. Desroches, A. Barthélémy, F. Louradour, and D. Pagnoux, "One shot endoscopic polarization measurement device based on a spectrally encoded polarization states generator," Opt. Express **23**, 16439–48 (2015).
[27] J. Fade and M. Alouini, "Depolarization remote sensing by orthogonality breaking," Phys. Rev. Lett. **109**, 043901 (2012).
[28] E. Schaub, J. Fade, N. Ortega-Quijano, C. Hamel, and M. Alouini, "Polarimetric contrast microscopy by orthogonality breaking," J. Opt. **16**, 122001 (2014).
[29] N. Ortega-Quijano, J. Fade, E. Schaub, F. Parnet, and M. Alouini, "Full characterization of dichroic samples from a single measurement by circular polarization orthogonality breaking," Opt. Lett. **40**, 1270–3 (2015).
[30] S. Jiao, W. Yu, G. Stoica, and L. V. Wang, "Contrast mechanisms in polarization-sensitive Mueller-matrix optical coherence tomography and application in burn imaging," Appl. Opt. **42**, 5191–7 (2003).
[31] B. H. Park, M. C. Pierce, B. Cense, and J. F. de Boer, "Jones matrix analysis for a polarization-sensitive optical coherence tomography system using fiber-optic components," Opt. Lett. **29**, 2512–4 (2004).
[32] C. Brosseau, *Fundamentals of polarized light: A statistical optics approach* (Wiley, 1998).
[33] S.-Y. Lu and R. A. Chipman, "Interpretation of Mueller matrices based on polar decomposition," J. Opt. Soc. Am. A **13**, 1106–13 (1996).
[34] M. I. Mishchenko, J. W. Hovenier, and L. D. Travis, *Light scattering by nonspherical particles* (Academic, 2000).
[35] V. V. Tuchin, L. V. Wang, and D. A. Zimnyakov, *Optical polarization in biomedical applications* (Springer, 2006).
[36] M. Alouini, F. Goudail, N. Roux, L. Le Hors, P. Hartemann, S. Breugnot, and D. Dolfi, "Active spectropolarimetric imaging: signature modeling, imaging demonstrator and target detection," Eur. Phys. J. Appl. Phys. **42**, 129–139 (2008).
[37] L. Pouget, J. Fade, C. Hamel, and M. Alouini, "Polarimetric imaging beyond the speckle grain scale," Appl. Opt. **51**, 7345–56 (2012).
[38] R. A. Chipman, "Mueller matrices," in *Handbook of Optics*, Vol. I, M. Bass, ed. (McGraw-Hill, 2010).
[39] D. G. M. Anderson and R. Barakat, "Necessary and sufficient conditions for a Mueller matrix to be derivable from a Jones matrix," J. Opt. Soc. Am. A **11**, 2305–19 (1994).
[40] K. V. Mardia and P. E. Jupp, *Directional Statistics* (Wiley, 1999).
[41] S. R. Cloude, "Group theory and polarisation algebra," Optik **75**, 26–36 (1986).
[42] J. J. Gil and E. Bernabeu, "A depolarization criterion in Mueller matrices," Opt. Acta **32**, 259–61 (1985).
[43] R. A. Chipman, "Depolarization index and the average degree of polarization," Appl. Opt. **44**, 2490-5 (2005).
[44] R. Ossikovski, "Alternative depolarization criteria for Mueller matrices," J. Opt. Soc. Am. A **27**, 808–14 (2010).
[45] N. Ortega-Quijano, F. Fanjul-Vélez, and J. L. Arce-Diego, "Physically meaningful depolarization metric based on the differential Mueller matrix," Opt. Lett. **40**, 3280–3 (2015).
[46] D. S. Kliger, J. W. Lewis, and C. E. Randall, *Polarized light in optics and spectroscopy* (Academic, 1990).